Supporting Information for "Detection and characterization of concentric expanding UV-emission observed in Jupiter's polar auroral regions"

V. Hue[1] *, T. K. Greathouse[1], G. R. Gladstone[1,2], B. Bonfond[3], J.-C. Gérard[3], M. F. Vogt[4], D. C. Grodent[3], M. H. Versteeg[1], J. A. Kammer[1], G. Clark[5], R. W. Ebert[1], R. S. Giles[1], M. W. Davis[1], K. Haewsantati[3,6,7], S. J. Bolton[1], S.M. Levin[8], J.E.P. Connerney[9,10]

[1]Southwest Research Institute, San Antonio, Texas, USA

[2]University of Texas at San Antonio, San Antonio, Texas, USA

[3]STAR Institute, LPAP, Université de Liège, Liège, Belgium

[4]Center for Space Physics, Boston University, Boston, MA, USA

[5]Johns Hopkins University Applied Physics Laboratory, Laurel, MD, USA

[6]Ph.D. program in Physics, Department of Physics and Materials Science, Faculty of Science, Chiang Mai University, Chiang Mai, Thailand

[7]National Astronomical Research Institute of Thailand (Public Organization), Chiang Mai, Thailand

[8]Jet Propulsion Laboratory, Pasadena, California, USA

[9]Space Research Corporation, Annapolis, MD 21403, USA

[10]NASA Goddard Spaceflight Center, Greenbelt, MD 20771, USA

*vhue@swri.edu

Contents of this file

1. Figures S1 to S7

Additional Supporting Information (Files uploaded separately)

1. Movies S1 to S4

Introduction

The additional information provided in this document concerns the different features presented and characterized in the publication. Figures S1 and S2 display additional details about the features detected on PJ9 and PJ12 in a similar fashion as those recorded during PJ4 and PJ6 and presented on Fig. 1 and Fig. 2 of the publication. The information is presented the same way as those in the publication, *i.e.,* an overview of the detected auroral emission on a single Juno-UVS swath, a set of plots showing the temporal evolution of the emission over consecutive spins, and the evolution of the brightness distributions of the feature.

Additionally, 4 animated movies are provided showing the evolution of the 4 events discussed in this paper, using a false-color imaging scheme. This scheme was used in previous publication [e.g., *Mauk et al., 2017*]. The animations show the brightness recorded in three spectral ranges and translated into false-colored red-green-blue channels. This gives information about the energy of the precipitating electron, going from high, medium to low, for the red, green and blue channels, respectively.

Figure S3 shows an example of the domain of validity in the magnetospheric mapping model of Vogt et al. (2011, 2015) for the PJ9 event discussed here. The format is similar to the one presented on the Vogt et al. papers, i.e., line colors indicate radial distance, and dots show noon/dawn/dusk/midnight. The 180° longitude is to the bottom of the

page. **In the PJ9 case, the event lies beyond the model validity which is constrained by the extend of the Galileo data fit. An estimate of the mapping beyond the region of model validity can however be obtained by assuming the field bendback continues smoothly and the radial field fall off beyond the magnetopause/beyond 150 $\mathbf{R}_J$.** Figures S4, S5, S6 and S7 display the extended radial distance and local time magnetospheric mapping results of the auroral features discussed. All but PJ12 use that approximation to map beyond the model validity. The plots show the typical magnetospheric mapping contours of Vogt et al. (2011, 2015) for subsolar longitudes auroral features were detected at. The feature location is shown by a black star. For the northern hemisphere, the subsolar point is directed at the bottom of the page. For the southern hemisphere, the subsolar longitude is directed to the top of the page and the plot is viewed from below the planet.

Movie S1

False-colored animation of the PJ4 event recorded on 2 Feb 2017 from 13:55:22 to 13:56:23, similar to the event presented on Fig. 1 of the publication.

Movie S2

False-colored animation of the PJ6 event recorded on 19 May 2017 from 05:06:48 to 05:08:49, similar to the event presented on Fig. 2 of the publication.

Movie S3

False-colored animation of the PJ9 event recorded on 24 Oct 2017 from 17:06:02 to 17:07:33, similar to the event presented on S1.

Movie S4

False-colored animation of the PJ12 event recorded on 1 Apr 2018 from 09:07:46 to 09:09:18, similar to the event presented on S2.

Occurrence rate of concentric expanding UV-emission in Jupiter

We provide here an estimate of the occurrence rate of these emission in Jupiter. The arguable minimum criteria in order for UVS to detect such feature in a given part of the atmosphere is to observe a ∼1000km-wide region for at least two consecutive spins. This can be done only when Juno was located below a certain altitude which would provide UVS high enough spatial resolution to distinguish them. We only selected data when UVS was below 1.4 R_J, which corresponds to a spatial resolution at nadir of ∼175 km. We therefore went through the Juno-UVS data used here and selected all the regions that fulfill these criteria. Only selecting ∼1000km-wide patches allows removing part of the data located near the edges of the slit or close to data gaps where these emissions would be difficult to identify. Additionally, only the regions of the polar aurora mapping to distances beyond 90 R_J have been selected using the model of Vogt et al. (2015).

An example is provided on Fig. S8 for PJ5 (27 March 2017), showing the time coverage during PJ5 of all selected observations fulfilling the aforementioned criteria (left) and the amount of time that magnetically maps beyond 90 R_J only (right). The time coverage is defined as follow: a given ∼1000km-wide patch that has been observed over two consecutive spins (∼30 seconds apart) is attributed an individual temporal coverage. That time is calculated given the derived properties of the feature. The averaged expanding veloc-

ity derived here is taken as 5.5 km/s, and we consider that they expands in averaged over ∼600km in radius between two consecutive spins. This means that such features have an averaged lifetime of 600/5.5 = 109 seconds, *i.e.,* more than 3 spins. We therefore consider that for each pair of consecutive spins over the same region effectively probes ∼109 seconds. This procedure was carried out for all consecutive set of spins, from PJ1 until PJ25, and the global temporal coverage map combining these is shown on Fig. S9. Note that, although the northern hemisphere becomes increasingly less visible to UVS as the mission goes, the altitude of Juno over the southern hemisphere evolves drastically once past PJ, which prevents UVS from observing the auroral features discussed here as easily than in the north.

Finally, considering the 3 events detected in the north and 1 in the south, we present an occurrence map of these features on Fig. S10. If we assume they follow a Poissonian statistics, the probability that one event is detected over an interval of time T is: $r\,T\,\exp(-r\,T)$, where r is the number of events per unit of time. The maximum likelihood for a single event to occur within an interval T is therefore given by $1/T$. In the north, the occurrence rate ranges from 1.4 to 2.6 events per Jovian day, while in the south it ranges from 3.4 to 3.9 events per Jovian day. Due to the low number of detection and the assumptions made to calculate the temporal coverage, these numbers should not represent a stringent constraint on the occurrence rate of these auroral features.

References

Bonfond, B., Grodent, D., Gérard, J. C., Stallard, T., Clarke, J. T., Yoneda, M., ... Gustin, J. (2012, January). Auroral evidence of Io's control over the magnetosphere of Jupiter. *Geophys. Res. Lett.,*, *39*(1), L01105. doi: 10.1029/2011GL050253

Vogt, M. F., Bunce, E. J., Kivelson, M. G., Khurana, K. K., Walker, R. J., Radioti, A., ... Grodent, D. (2015, April). Magnetosphere-ionosphere mapping at Jupiter: Quantifying the effects of using different internal field models. *Journal of Geophysical Research (Space Physics)*, *120*(4), 2584-2599. doi: 10.1002/2014JA020729

Vogt, M. F., Kivelson, M. G., Khurana, K. K., Walker, R. J., Bonfond, B., Grodent, D., & Radioti, A. (2011, Mar). Improved mapping of Jupiter's auroral features to magnetospheric sources. *Journal of Geophysical Research (Space Physics)*, *116*(A3), A03220. doi: 10.1029/2010JA016148

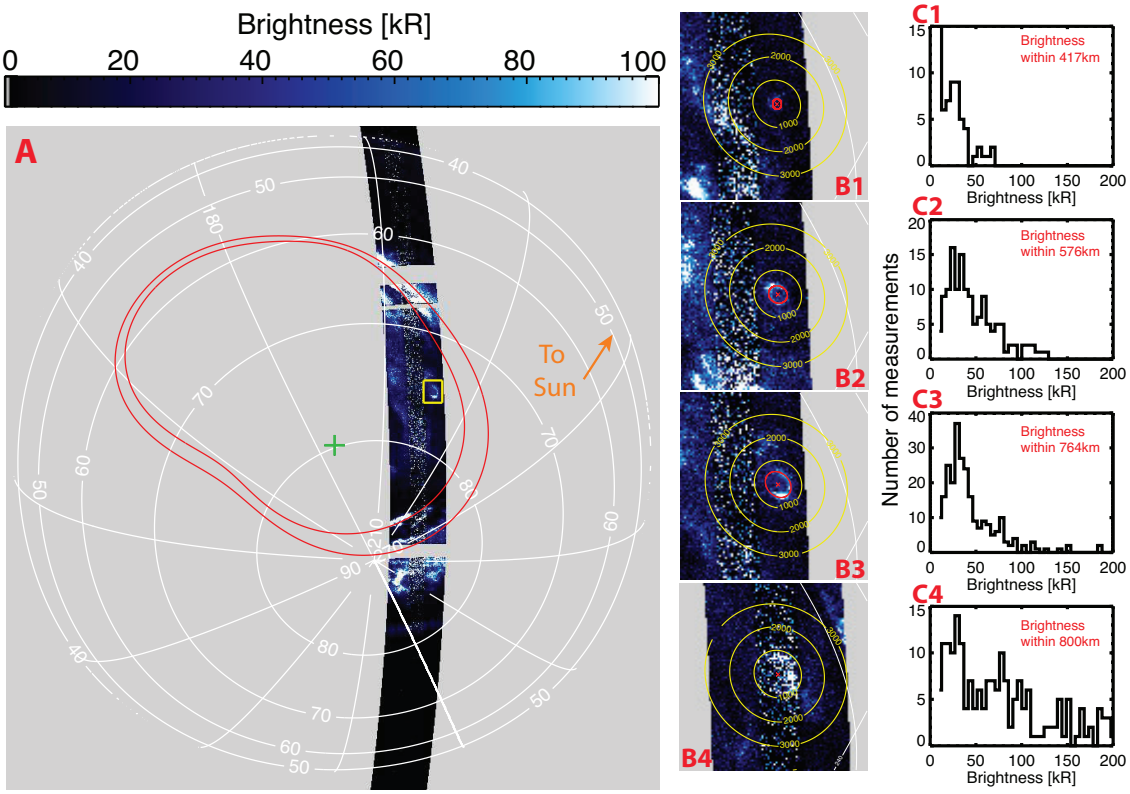

Figure S1. New feature detected on 24 Oct 2017 from 17:06:02 to 17:07:33, during PJ9 in the northern polar auroral region. Panel A: overview of the detected auroral emission over a single Juno-UVS swath. **The green cross represent the sub-Juno position at the median detection time.** Panels B: Evolution of the detected feature over consecutive spins. The red cross indicates the center of the feature, while the yellow contours shows the distance of every pixel to the center of the feature. An ellipse fit is performed on sub-panels B2 and B3, and the brightness distributions of the feature is shown on sub-panels C2 and C3. No simultaneous Juno in-situ measurements are available at the time this feature was detected.

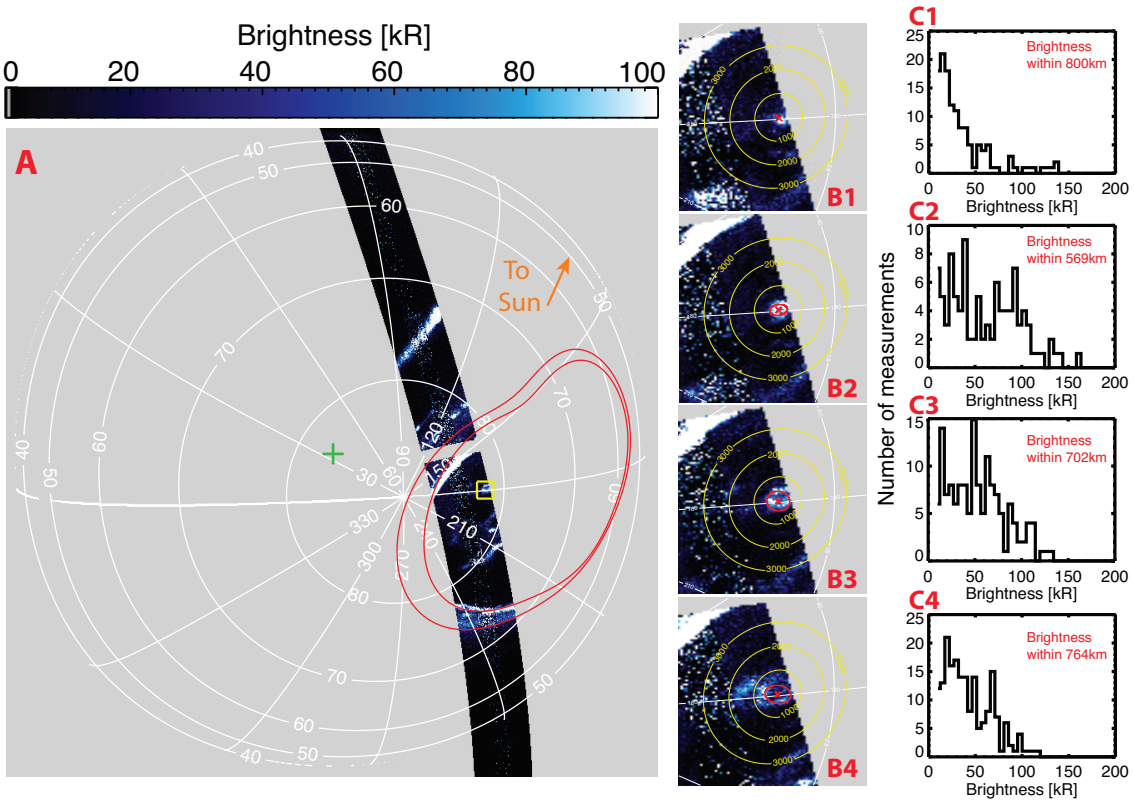

Figure S2. Same as S1 for the event detected during PJ12 on 1 Apr 2018 from 09:07:46 to 09:09:18. No simultaneous Juno in-situ measurements are available at the time this feature was detected.

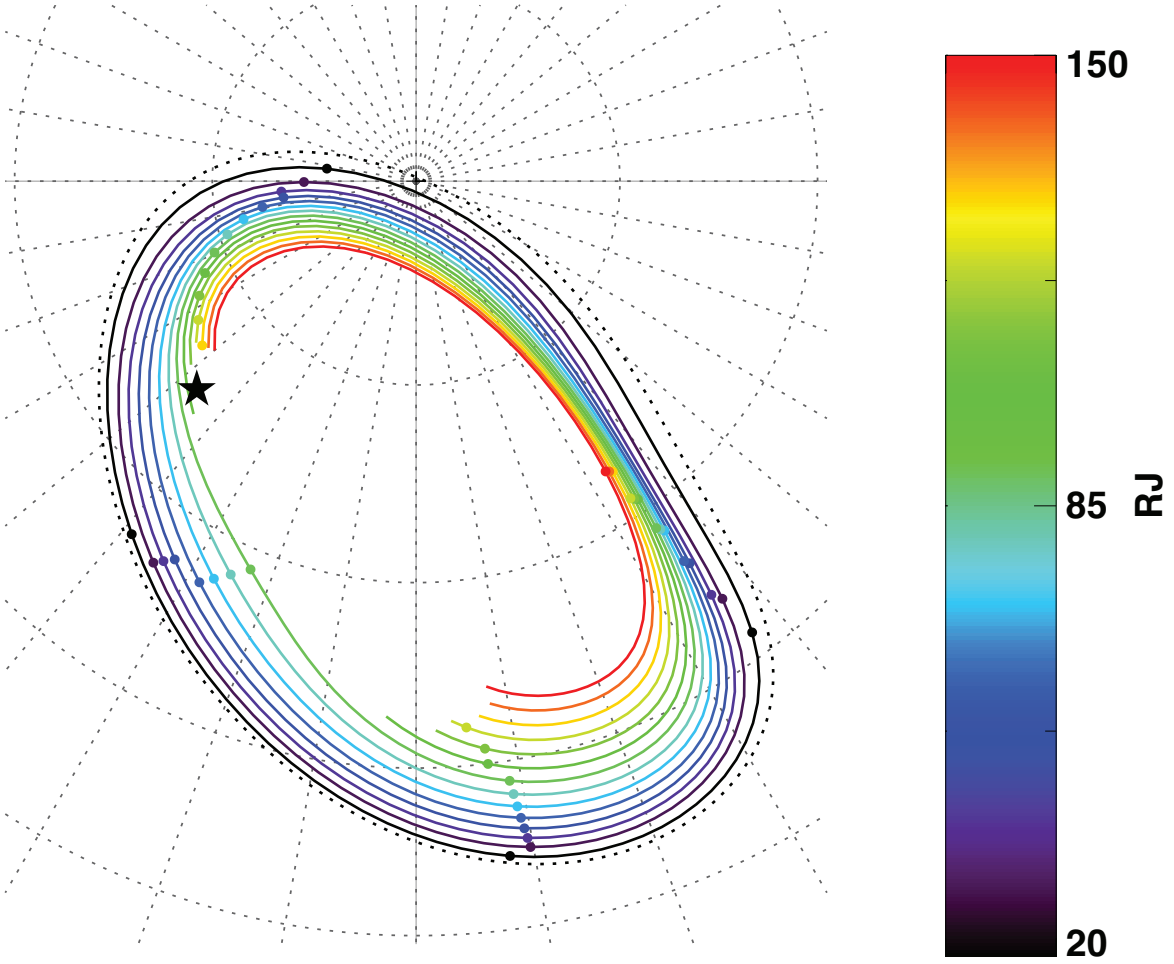

Figure S3. Limitation of the magnetospheric mapping at the time the PJ9 aurora feature was detected. The mapping contours show where the model of Vogt et al. (2011, 2015) is normally valid. The 180° longitude is to the bottom of the page. The detected feature maps beyond the model validity.

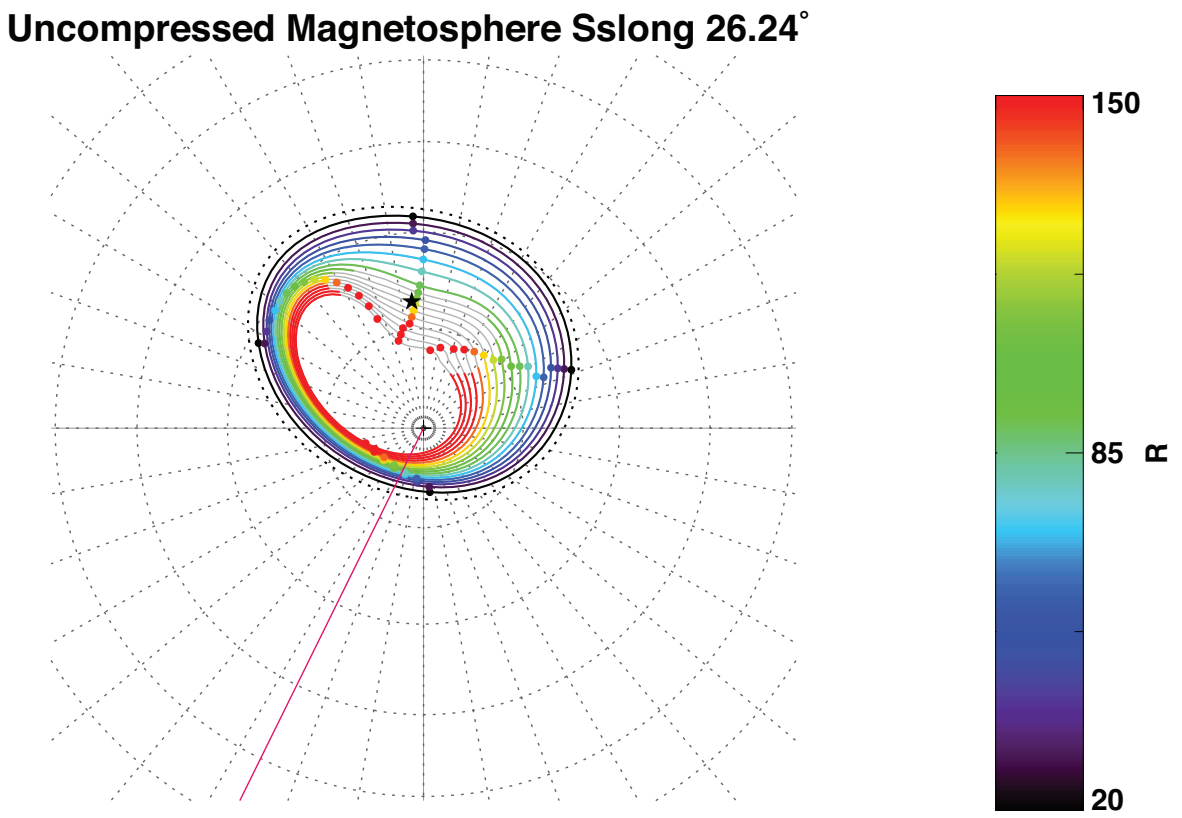

Figure S4. Magnetospheric mapping at the time the PJ4 aurora feature was detected, according to the model of Vogt et al. (2011, 2015). The feature location is shown by a black star. Dusk is to the right and dawn is to the left, and the pink line drawn at S3 W-longitude 180° for reference. The subsolar point is directed to the top of the page and the plot is viewed from below the planet.

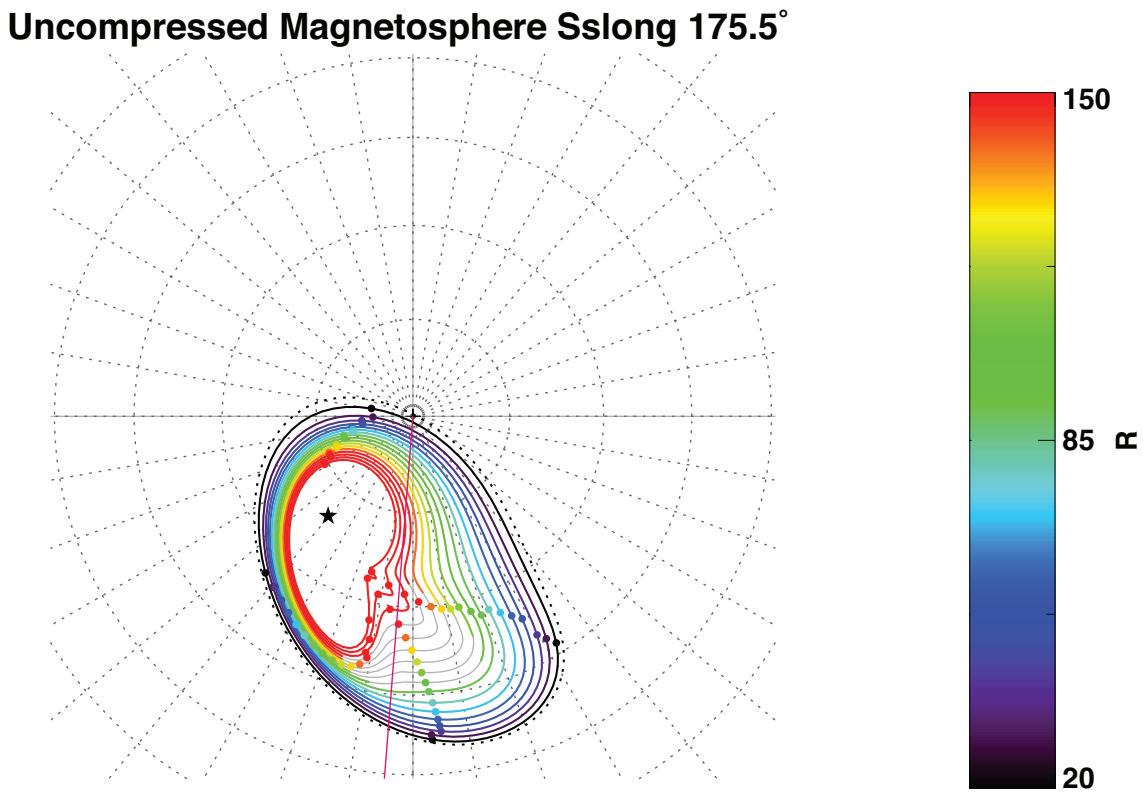

Figure S5. Same as Fig. S4 for the auroral feature detected during PJ6. The subsolar point is directed to the bottom of the page.

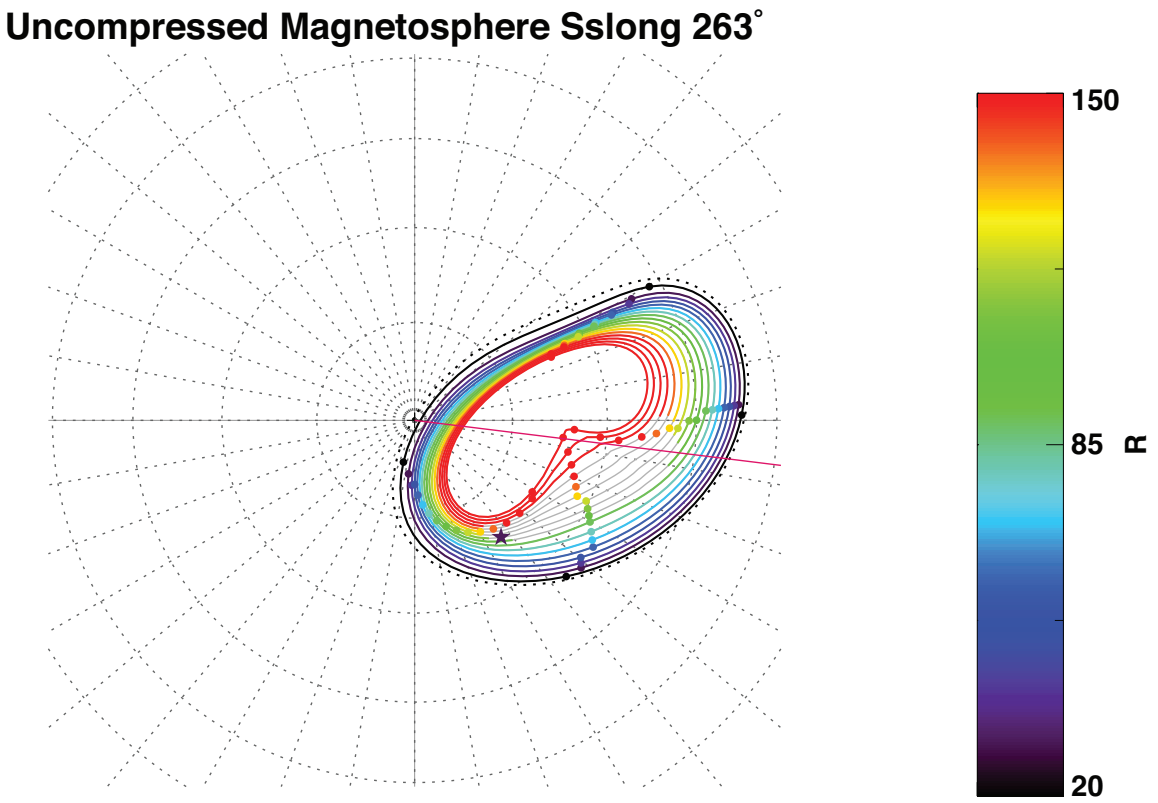

Figure S6. Same as Fig. S4 for the auroral feature detected during PJ9. The subsolar point is directed to the bottom of the page.

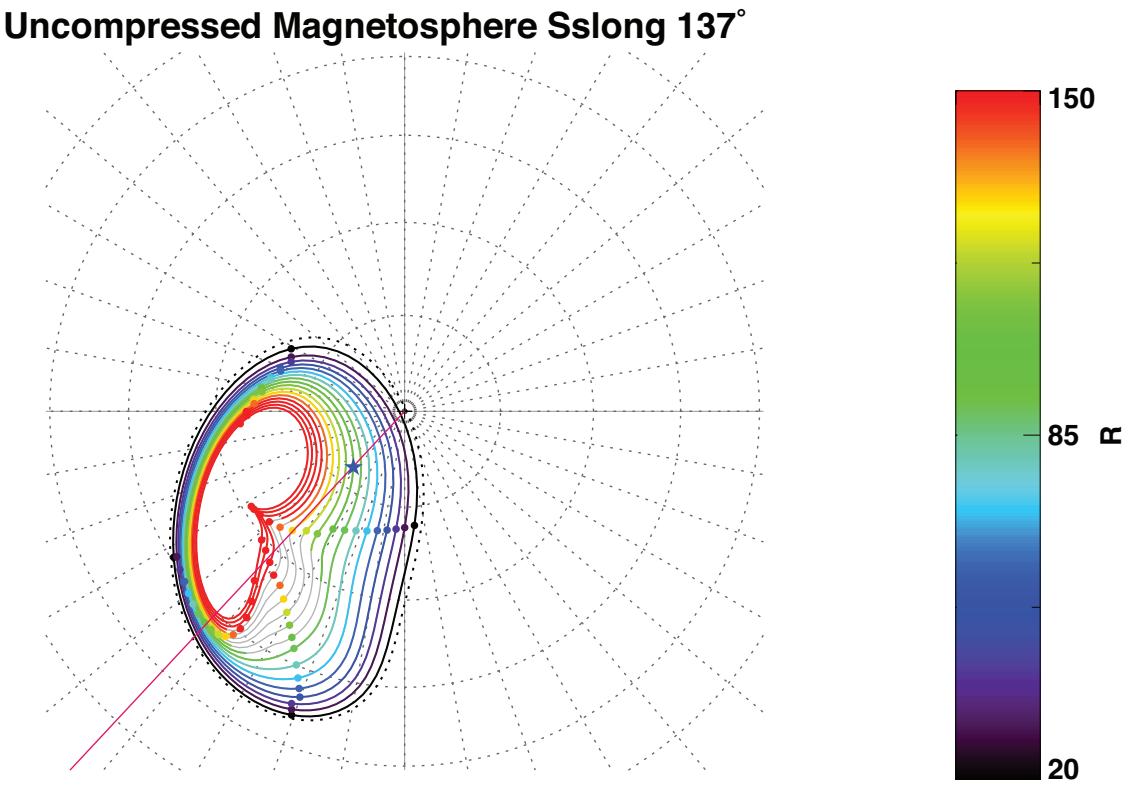

Figure S7. Same as Fig. S4 for the auroral feature detected during PJ12. The subsolar point is directed to the bottom of the page.

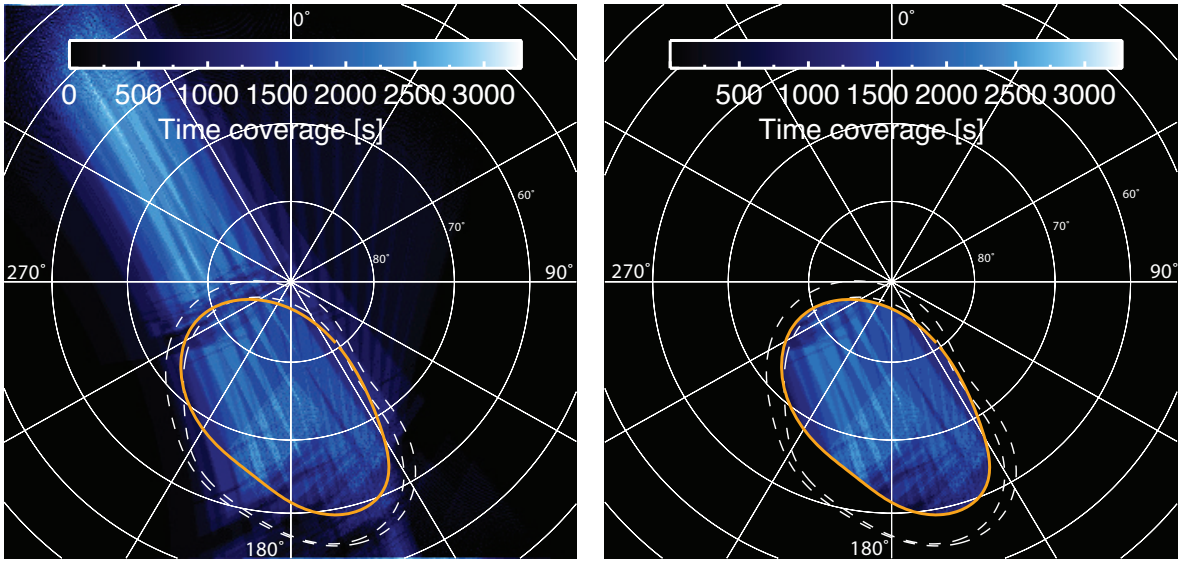

Figure S8. Temporal coverage (see text) for PJ5 (27 March 2017). Left: temporal coverage map of all selected observations with potential expanding auroras detectability. Right: selection of the region mapping to beyond 90 R_J using the model of Vogt et al. (2015). White dashed line: reference ovals from Bonfond et al. (2012). Orange line: magnetodisk mapping distance of 90 R_J.

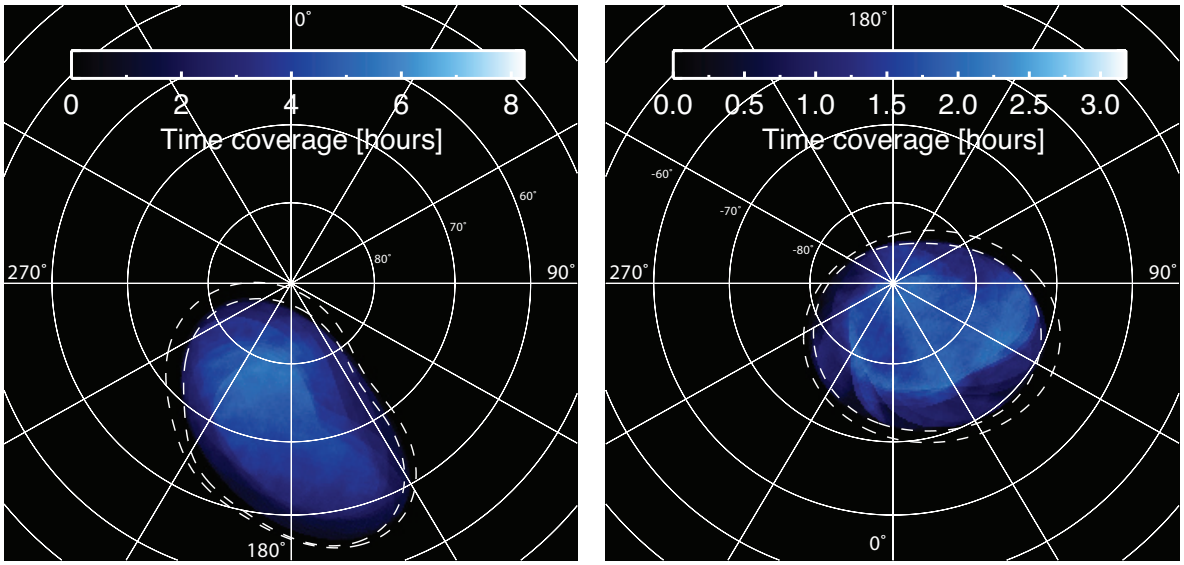

Figure S9. Global time coverage maps in the north (left) and south (right) combining PJ1 up to PJ25 included. Note the different colorbar on each plots.

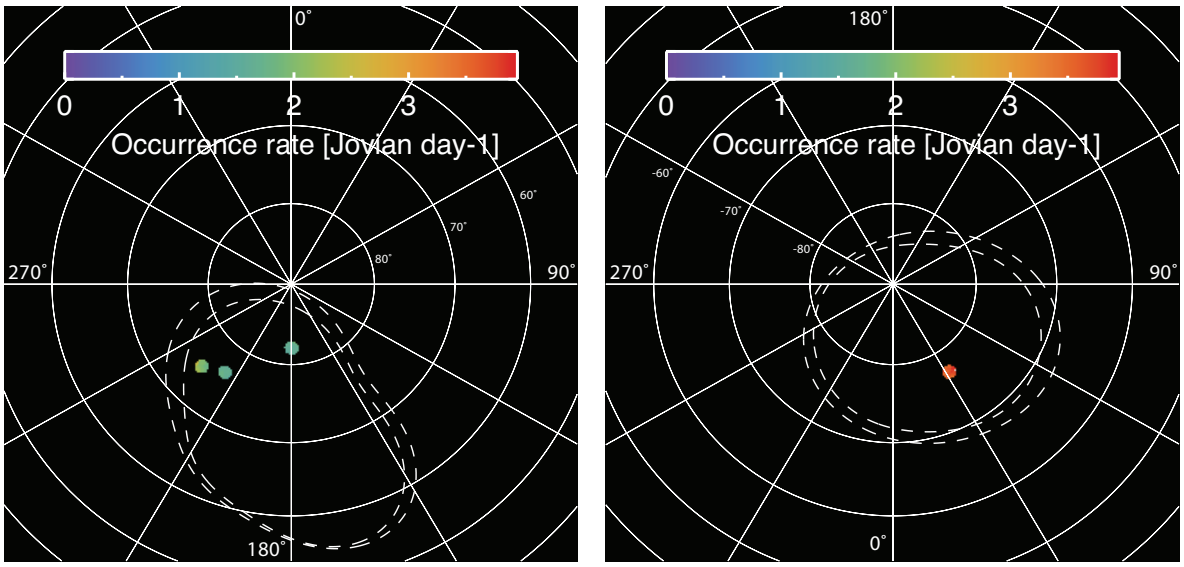

Figure S10. Occurrence rate of expanding aurora in the north (left) and the south (right), combining from PJ1 up to PJ25 data.